JCTC Journal of Chemical Theory and Computation

Article

pubs.acs.org/JCTC

Multiconfigurational Second-Order Perturbation Theory with Frozen Natural Orbitals Extended to the Treatment of Photochemical Problems

Javier Segarra-Martí,[*,†] Marco Garavelli,[*,†,‡] and Francesco Aquilante[*,†]

[†]Dipartimento di Chimica "G. Ciamician", Università di Bologna, Via Selmi 2, IT-40126 Bologna, Italy

[‡]Université de Lyon, CNRS, Institut de Chimie de Lyon, École Normale Supérieure de Lyon, 46 Allée d'Italie, F-69364 Lyon Cedex 07, France

ABSTRACT: A new flavor of the frozen natural orbital complete active space second-order perturbation theory method (FNO-CASPT2, Aquilante et al., *J. Chem. Phys.* **131**, 034113) is proposed herein. In this new implementation, the virtual space in Cholesky decomposition-based CASPT2 computations (CD-CASPT2) is truncated by excluding those orbitals that contribute the least toward preserving a predefined value of the trace of an approximate density matrix, as that represents a measure of the amount of dynamic correlation retained in the model. In this way, the amount of correlation included is practically constant at all nuclear arrangements, thus allowing for the computation of smooth electronic states surfaces and energy gradients—essential requirements for theoretical studies in photochemistry. The method has been benchmarked for a series of relevant biochromophores for which large speed-ups have been recorded while retaining the accuracy achieved in the corresponding CD-CASPT2 calculations. Both vertical excitation energies and gradient calculations have been carried out to establish general guidelines as to how much correlation needs to be retained in the calculation for the results to be consistent with the CD-CASPT2 findings. Our results feature errors within a tenth of an eV for the most difficult cases and have been validated to be used for gradient computations where an up to 3-fold speed-up is observed depending on the size of the system and the basis set employed.

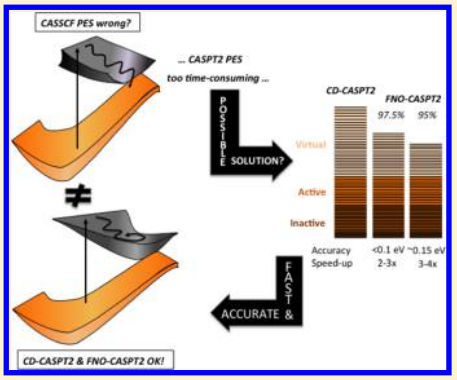

1. INTRODUCTION

Nondynamical electron correlation effects are of paramount importance to properly describe the electronic structure of molecules. Countless efforts have been carried out over the years to include these subtle yet sometimes strongly pronounced effects,[1−6] whose importance cannot be overstated, especially when dealing with electronic excited states often exhibiting a multiconfigurational nature.[7,8] These states and the photo-induced events triggered upon their population usually involve different photophysical and photochemical phenomena taking place close to interstate intersections mediating nonradiative intersystem crossing and internal conversion processes. At the vicinity of these crossing regions, the nature of the excited state is that of mixed character, thus requiring a multiconfigurational treatment that smoothly accounts for the sharp deviations in nature typical of these regions. A natural starting point for tackling these issues relies on the formulation of a multi-configurational wave function with the complete active space self-consistent field (CASSCF) wave function being the most popular choice.[1,3−5,9,10] Within the CASSCF model, non-dynamical correlation is included by building a wave function that spans the space of all possible configurations for a specified set of electrons distributed among a certain number of orbitals selected to address a specific problem (so-called active space).[11]

Despite the exponential scaling of the number of parameters that needs to be determined when working with a CASSCF ansatz, it is quite remarkable the amount of chemical problems that can be studied qualitatively with just an active space that contains a handful of electrons and orbitals. Especially noteworthy in this respect are the latest efforts in adapting the density matrix renormalization group (DMRG)[12] techniques to solve the Full Configuration Interaction problem,[13,14] providing major speed-ups that allow the computation of over 30 electrons in as many orbitals in the active space, as well as the most recent results on graphically contracted functions as an alternative way to solve the problem.[15,16] Quantitative studies are in fact beyond the reach of CASSCF. Indeed, although CASSCF accounts for the nondynamical (also known as static) correlation of the system, at this level of theory, negligible is the accounted contribution to the dynamical correlation arisen due to the correlated motion of the electrons.[17] An alternative way to introduce approximate CASSCF-type wave functions with a certain degree of dynamic correlation is provided by the recently introduced split-gas method,[18,19] which appears to be more computationally affordable.

In the attempt to add dynamical correlation effects on top of a multiconfigurational wave function, several approaches have been devised over the years based on a variety of ideas. These can be mainly framed within several big groups depending on

Received: May 22, 2015
Published: July 22, 2015

DOI: 10.1021/acs.jctc.5b00479
J. Chem. Theory Comput. 2015, 11, 3772−3784

whether the correlation is added perturbationally,[20−27] through a coupled-cluster ansatz,[28−31] within a configuration interaction approach,[5,32,33] employing density functional theory (DFT)-based[34,35] techniques, or within a canonical transformation-based approach.[36,37] Those based upon a perturbational treatment on top of the CASSCF wave function—like the ones that will be discussed in the present work—are the most popular choice due to their relatively low computational cost relative to the quality of the results obtained, compared to the more computationally expensive and accurate approaches mentioned above. Particularly popular is the method based on second-order Møller−Plesset (MP) perturbation theory widely known as CASPT2,[21,22,24−27,38,39] as well as its different multistate and extended multistate formulations,[40−42] the latter providing more accurate estimates for regions of near degeneracy where two or more configuration state functions are to be accounted for in the reference wave function. These methods have been widely employed over the last two decades to tackle a series of spectroscopic and photochemical problems, yet their relatively large cost relative to other single-reference methods have hindered their usage for larger-sized and more realistic molecules. Several computationally efficient approximations have been proposed over the years to overcome this hurdle, the most employed being based on a density fitting or Cholesky decomposed scheme[43,44] to reduce the cost of the two-electron integrals as well as the cost associated with CASPT2 in what has been coined CD-CASPT2[45,46] or DF-CASPT2.[47]

Whereas these variants of CASPT2 achieve a much better computational efficiency, they are still far from being cheap enough to be used in routine optimizations or for vertical excitation energies in moderately large systems or for accurate basis sets. To tackle this issue, a new variant of the CD-CASPT2 was introduced in which a fraction of the secondary orbitals can be effectively excluded from the perturbation step.[48] It should be noted that this translates into a quadratic reduction in the number of unknown amplitudes to be determined, as for a system containing O inactive + active orbitals, and V active + virtual orbitals, the total number of amplitudes is in fact $\sim O^2V^2$.

This type of approximation has been widely employed over the years for single-reference methods and is mainly based on the pioneering work of Pulay and co-workers[49−51] as well as others,[52,53] where localized natural orbitals (NOs)[54] were employed to reduce the computational cost by truncating the virtual space and thus removing the contributions of a fraction of the virtual orbitals in the correlation step.[55−60] These methods have nowadays regained popularity, being formulated through pair natural orbital (PNO), local pair natural orbital (LPNO), and domain-based local pair natural orbital (DLPNO) approximations,[61−66] as well as through explicitly correlated local methods[67−69] or by employing the orbital-specific virtual (OSV) approach.[70−72] This list is by no means exhaustive as the field has dramatically progressed over the last two decades, being mainly applied to single-reference coupled-cluster and second- and third-order MP ground state methods, even though some recent implementations on CC2 and ADC(2) have been reported,[73−75] as well as the first, to our knowledge, PNO implementation for multireference coupled-cluster.[76]

The particular approximation to be employed in the present manuscript, based on the frozen natural orbital (FNO) approach, was introduced in the seventies.[77] The approach taken was to employ a natural orbital configuration interaction reference wave function and perform approximate second-order perturbation theory on only a fraction of the space spanned by the natural orbitals, excluding the highest-lying and less important NOs from the perturbative step, thus drastically reducing the computational cost. This technique has been widely employed in many-body perturbation theory methods,[78] especially for coupled-cluster, where it registers larger speed-ups due to its iterative nature.[79] In 2009, this method was extended to the CASPT2 method (FNO-CASPT2),[48] employing the ideas previously introduced for restricting the number of transitions to the virtual space within a CASPT2 framework. It has been successfully employed ever since to study comparatively larger systems with very accurate basis sets while retaining a similar accuracy as that expected by the CD-CASPT2 method. Nevertheless, the method's general applicability is severely restricted by the way it selects the secondary orbitals to be trimmed from the perturbational treatment, as they are chosen automatically to be the highest-lying in the secondary space. This leads to an uneven accounting of the correlation energy for different nuclear arrangements, as the position and shape of the orbitals in the secondary space is geometry dependent and therefore the orbitals excluded from the perturbation are different, retaining a different amount of correlation depending on the geometry and thus being inadequate for its usage in common photoinduced computational schemes, such as dissociation curves or geometry/minimum energy path optimizations.

In this contribution, we present an implementation of the FNO procedure that employs similar concepts to those extensively used in the FNO and CSV schemes,[61,70] where the orbitals to be excluded from the perturbation treatment are selected in terms of their contribution to the trace of the reduced density matrix, yielding a consistent and general criteria that retains an analogous amount of correlation for different nuclear arrangements, thus allowing its use for photophysical and photochemical studies. A certain percentage of the trace of the reduced density matrix is specified by the user, and the orbital exclusion is carried out by removing the higher-lying diffuse and less important orbitals until the percentage of the reduced density matrix required is achieved, this being directly related to the amount of correlation preserved in the calculation with respect to the CD-CASPT2 solution. The importance of mapping the excited-state hypersurfaces at the dynamically correlated CASPT2 level instead of the usually employed CASSCF cannot be overstated, and a couple examples are given here to highlight this issue. The commonly used CASPT2//CASSCF approach, in which surfaces are mapped at the CASSCF level whereas single-point energy corrections are given using CASPT2, has a wide applicability but fails to treat some systems in which the CASSCF and CASPT2 surfaces do not evolve in parallel. Moreover, recent theoretical studies have shed some doubts on the general applicability of the protocol, which has been shown to fail in cases where dynamic correlation plays an important role, such as those arising from intermolecular interactions or due to an uneven treatment of the different excited states partaking in the photoprocess. To cover this issue, a CD-CASPT2//FNO-CASPT2 protocol is suggested here, making use of the computationally cheaper FNO-CASPT2 to map the potential energy hypersurfaces while adding a single-point correction at the CD-CASPT2 if needed. The method is thoroughly benchmarked for its usage in computing vertical excitation energies, gradients, and dissociation curves, being the main tools employed in theoretical photochemistry. The results here obtained endorse the use of the FNO-CASPT2 technique

DOI: 10.1021/acs.jctc.5b00479
J. Chem. Theory Comput. 2015, 11, 3772−3784

to routinely track the excited state evolution in static as well as in molecular dynamics simulations, yielding analogous results to those obtained at the CD-CASPT2 level while providing an up to 4× speed-up in the calculations, making them feasible.

2. THEORY

The excitations manifold used to define the CASPT2 model is often subdivided in three subgroups identified by the number of virtual orbitals, zero, one, or two, to which electrons are excited, namely in the submanifolds[21]

Internal	Semi-internal	External
	$\hat{E}_{atuv}$	$\hat{E}_{atbu}$
$\hat{E}_{tiuv}$	$\hat{E}_{aitu}$ or $\hat{E}_{tiau}$	$\hat{E}_{aibt}$
$\hat{E}_{tiuj}$	$\hat{E}_{tiaj}$	$\hat{E}_{aibj}$

where $\hat{E}$ indicates the (singlet) double excitation operator. The objective successfully achieved by the FNO-CASPT2 approach is to define and use, for the CASPT2 treatment, a smaller set of approximate NOs that effectively span the virtual space with respect to all semi-internal and external excitations reported above in a very similar fashion to its single-reference PNO and OSV counterparts.[61,64−66,72] By their nature, even approximate NOs allow a hierachical buildup of dynamical electron correlation.[54] A truncation of the virtual space—not possible in the canonical representation, as the resulting loss of accuracy is too severe[80]—can then be effective when such NOs are excluded based on the smallness of their occupation number. The transformation matrix that allows the space to go from the (pseudo)canonical orbitals to a particular class of NOs is defined as the one diagonalizing the following virtual−virtual block of the following MP2-type density matrix.[78,79]

$$\tilde{D}^{(2)}_{ab} = \sum_{ic} t^{ac}_{ii} t^{cb}_{ii} \tag{1}$$

with the amplitudes defined as

$$t^{ab}_{kk} = -\frac{(ak|bk)}{\epsilon_a + \epsilon_b - 2\epsilon_k} \tag{2}$$

The two-electron integrals included in eq 2 can be conveniently computed by means of their CD/DF representation,[45] namely

$$(ak|bk) = \sum_{J}^{M} L^{J}_{ak} L^{J}_{bk} \tag{3}$$

where the number of CD/DF vectors in typical applications is within the range of 3−5 times the number of basis functions.[46] The evaluation of $\tilde{D}^{(2)}$ is a fourth-order step (cost $\sim OV^3$) and, thanks to eq 3, so is the preliminary step of computing the needed amplitudes (cost $\sim OV^2M$). Therefore, no fifth-order steps are involved in the overheads for the FNO selection that would otherwise render the process as costly as the full CASPT2 calculation. Once these virtual orbitals have been selected, the standard virtual−virtual block of the Fock matrix used in CASPT2 is calculated and diagonalized in this smaller orbital space. Finally, an estimate of the truncation error can also be determined by using the standard expression for the canonical MP2 energy but restricted to the case of identical inactive orbital indices ($i = j$), namely

$$\tilde{E}_{\mathrm{MP2}} = -\sum_{iab} \frac{(ai|bi)^2}{\epsilon_a + \epsilon_b - 2\epsilon_i} \tag{4}$$

However, the corresponding correction to the energy $\Delta E_{\mathrm{MP2}} = E_{\mathrm{MP2}}[\mathrm{full}] - E_{\mathrm{MP2}}[\mathrm{truncated}]$ is only relevant for small basis and severe truncations. The virtual orbitals and orbital energies to be used in the truncated MP2 calculation can be obtained from the canonical orbital energies via diagonalization of the Fock matrix in the reduced virtual space,[77−79] $F = U\,\epsilon\,U^T$, where U is the orthogonal matrix of the eigenvectors of $\tilde{D}^{(2)}$. In the above equations, a particular treatment is deserved to the active orbitals (included in the sums with the less common notation i, j, ...). The need to access meaningful orbital energies in this subspace leads to the preference for pseudocanonical active orbitals, obtained by diagonalization of the active−active block of the CASSCF Fock matrix. Moreover, to mimic the occupied-virtual separation of single-reference wave functions,[61,65,66,70,72,79] these orbitals are then split into two subgroups on the basis of their eigenvalues. Only those corresponding to negative eigenvalues are retained in the definition of the density matrix of eq 1, and they are considered in the same way as the inactive orbitals, thus, as if they were doubly occupied.

However, successfully truncating the virtual space in the FNO-CASPT2[48] as well as in other FNO[78,79] and related methods[49−51] suffered from a major drawback: there is not a robust measure that could be used to predict the amount of correlation energy included for a given truncation of the orbital space. Despite the fact that satisfactory accuracy was achieved by truncating 50−60% of the virtual space, it also became clear that a smooth potential energy surface (PES) could not be guaranteed by a single choice of the retained fraction of NOs, as it has also been reported for related methods based on the same concept.[81−83] In fact, in the range 50−60%, a single value for the truncation would result in a different amount of correlation energy included along the PES. This issue can be partially solved for gradient computations by formulating a coupled-perturbed set of equations yielding an analytical solution as has been shown elsewhere,[79] even though the discontinuities in the PES are expected to remain if the geometrical changes are pronounced from one step to the next. In the present paper, we show that such shortcoming can be lifted by replacing the choice of the fraction of NOs with that of a specific estimator of the correlation energy included. The estimator chosen is the percentage of the trace of the density matrix defined in eq 1, namely

$$\%\mathrm{Tr} = 100\frac{\sum_a^{\nu} \eta_a}{Tr(\tilde{D}^{(2)})} \tag{5}$$

where the number of retained virtual NOs ν is determined by including more and more virtual NOs, preordered according to the decreasing occupation numbers η's (eigenvalues of $\tilde{D}^{(2)}$), until a chosen value of %Tr is reached. This estimator is different to the one employed for PNO methods, where the PNOs are retained in the calculation if $\eta \geq \tau_{\mathrm{CutPNO}}$, with τ_{CutPNO} being the threshold defined to keep the PNOs in the computation,[61] essentially a pair orbital-dependent adaptation of the standard FNO selection criterion.[78,79] The estimator used for the NO selection presented here is also independent of any possible localized nature of the orbitals. Despite some similarities, this fact also distances our method from the OSV protocol, where a domain of OSVs is generated based on the eigenvalues of the

DOI: 10.1021/acs.jctc.5b00479
J. Chem. Theory Comput. 2015, 11, 3772−3784

"diagonal" amplitudes.[70] The trace of the reduced density matrix is extensive with respect to the number of retained NOs and represents a measure of the amount of electronic charge that will populate the virtual space resulting from the correlation effects included at the CASPT2 level, being a suitable estimate of the correlation energy. The results of the extensive investigations present in the next section prove that a suitable threshold for % Tr can be chosen based on the sought accuracy such that it guarantees uniform accuracy along the PES.

3. RESULTS AND DISCUSSION

Four different molecular systems, widely known for their biological importance, have been selected to benchmark the present method and to provide guidelines for its usage in other biochromophores and related molecules of interest. Two of them are protonated Schiff bases of different sizes, PSB-3[84] and PSB-11,[85,86] another is the DNA nucleobase thymine,[87,88] and the last is the water dimer, which displays the smallest water aggregate presenting a hydrogen-boding motif.[89,90] Their molecular structures are shown in Figure 1. This variety of molecular systems has been chosen to test the capabilities of the new FNO-CASPT2 implementation in terms of (i) basis set dependence and relative speed-ups for vertical excitation energies, (ii) gradient computations, being tested through geometry optimizations by extracting the main geometrical parameters and comparing with respect to reference CD-CASPT2 results, and (iii) potential energy curves of dissociation processes to demonstrate the correct behavior of the new method in terms of its applicability and capabilities to map and describe excited-state-driven photophysical and photochemical processes.

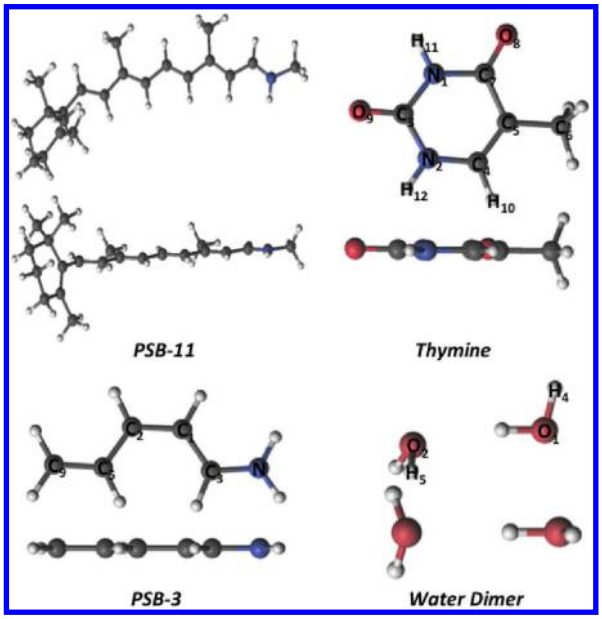

Figure 1. Equilibrium structures for the electronic ground state of the four molecules under study and their respective atomic labels.

All computations have been carried out on an in-house development version of the MOLCAS package.[91,92] Multiconfigurational wave functions have been initially determined at the CASSCF level, comprising all valence π occupied and unoccupied orbitals for the protonated Schiff bases (PSB), all valence π occupied and unoccupied plus the oxygen occupied lone-pair (n_O) orbitals for thymine, and the full valence shell for the water dimer. This accounts for six electrons in six orbitals (CASSCF(6,6)) for the smallest PSB-3, CASSCF(12,12) for PSB-11, CASSCF(14,10) for thymine, and CASSCF(16,12) for the water dimer. No symmetry restrictions have been imposed on the systems yielding an unconstrained approach, even though some of them might display a given spatial symmetry. A series of basis sets have been used: (i) a segmented basis set of the Pople-type 6-31G*,[93] and (ii) an atomic natural orbital (ANO) type within the large (ANO-L) primitive set[94,95] C,N,O(14s9p4d3f)/H(8s4p3d) contracted to C,N,O-[3s2p1d]/H[2s1p] (hereafter ANO-L 321/21) and to C,N,O-[4s3p2d]/H[2s1p] (hereafter ANO-L 432/21). Auxiliary basis sets for the density fitting have been used throughout based on the Cholesky decomposition technique.[43,44,96−98] An equal-weighting state average procedure of three, five, and seven was employed for both PSB systems, the water dimer, and thymine, respectively, in order to stabilize the active space and to account for all the important states being studied.

CASPT2 computations have been performed on top of the previously described CASSCF wave functions to account for the dynamic correlation.[21,22] All electrons in the core−shells have been kept frozen during the perturbation step. To minimize the effect of weakly interacting intruder states, an imaginary level-shift of 0.2 au has been employed.[99] No IPEA shift has been used in the CASPT2 computations.[100] The Cholesky-based CASPT2 method (CD-CASPT2),[45] which has been recently shown to provide a similar accuracy as that of the CASPT2 method,[46] has been used as a reference to benchmark the new implementation of the FNO-CASPT2[48] approach described here. Geometry optimizations have been carried out making use of numerical gradients for the different FNO- and CD-CASPT2 schemes used in this work and with analytical gradients at the CASSCF level.[101]

3.1. Vertical Excitation Energies. To assess the performance of the FNO-CASPT2 implementation presented here, the largest molecular systems under study, thymine and PSB-11, have been selected and benchmarked over a series of basis sets of increasing size. These molecular systems have been selected as the speed-up in the FNO-CASPT2 procedure is related to the removal of secondary orbitals in the perturbation step, therefore reducing the amount of amplitudes to be computed and thus being intimately linked with the size of the system and the diffusiveness of the basis set employed, providing larger computational gains for the larger molecular structures. These systems also provide a variety of excited-state transitions featuring highly covalent (i.e., $n_O\pi^*$), ionic (i.e., $\pi\pi^*$ in thymine), and highly ionic (i.e., $\pi\pi^*$ intramolecular charge transfer (ICT) in PSB-11) transitions, displaying an increasing dependence on the amount of dynamic correlation included by going from covalent to highly ionic states, covalent and ionic referring to hole−hole and hole−pair structures in valence bond theory, respectively.[102]

A variety of parameters associated with the computation of the vertical excitation energies have been analyzed, providing a broad picture of the capabilities of the new FNO-CASPT2 implementation and its behavior compared to CD-CASPT2 computations. Figures 2 and 3 depict the results obtained for thymine and PSB-11, respectively. The main parameters analyzed are based on the evolution of the vertical excitation energies for a wide range of FNO schemes retaining diverse percentages of the trace of the density matrix and thus preserving a fraction of the dynamic correlation added perturbationally. The related computational savings are analyzed

DOI: 10.1021/acs.jctc.5b00479
J. Chem. Theory Comput. 2015, 11, 3772−3784

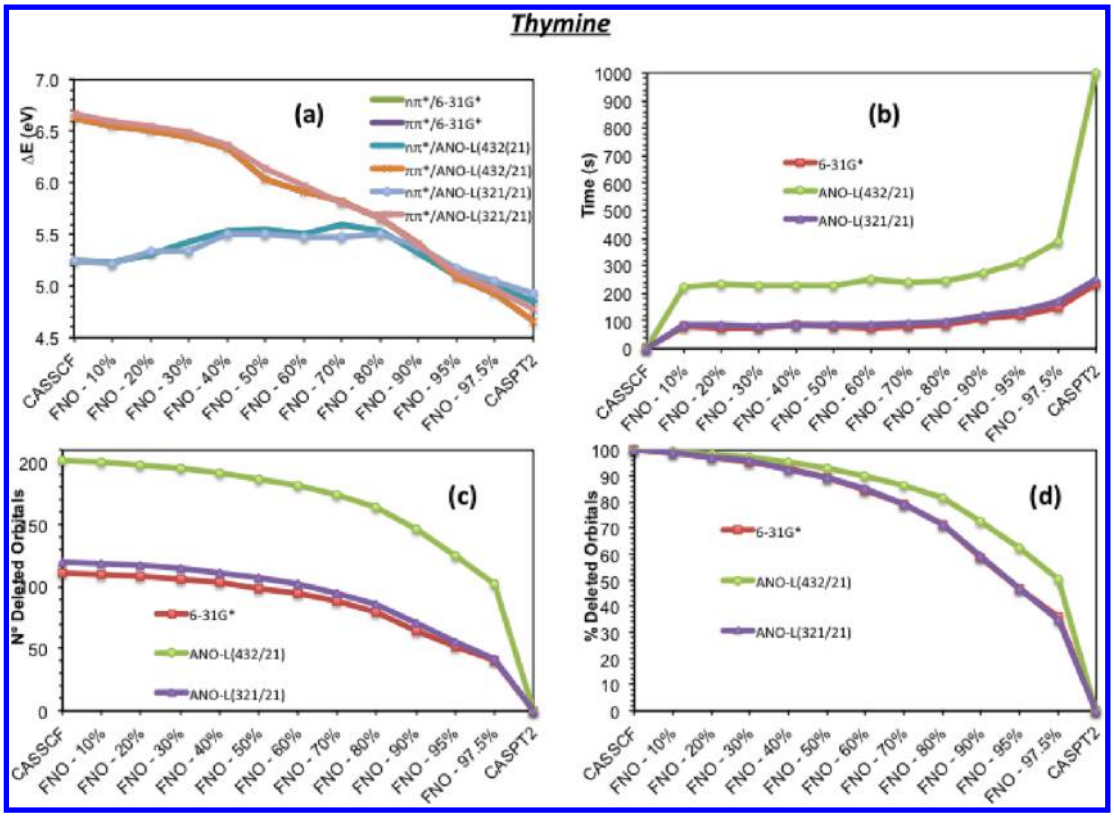

Figure 2. FNO-CASPT2 vs CD-CASPT2 benchmark for thymine: (a) vertical excitation energies (ΔE, in eV) for the different FNO schemes and the lowest-lying $n_O\pi^*$ and $\pi\pi^*$ excited states, (b) timings (in s) for the computation of the lowest-lying 7 states of the diverse FNO-CASPT2 calculations with respect to the CD-CASPT2 reference (see text), (c) number of secondary orbitals deleted in the perturbation step, and (d) percentage of the total secondary space deleted in each calculation.

in terms of the time required to carry out the computations, as well as based on the number and percentage of deleted secondary orbitals in the perturbation step for the different FNO schemes depicted.

For thymine, the lowest-lying $n_O\pi^*$ and $\pi\pi^*$ electronic excited states have been computed with respect to a variety of FNO-CASPT2 approaches and to the CD-CASPT2 solution. Figure 2 shows the different trends obtained for the two distinct excited states analyzed by increasing the dynamic correlation energy by going from CASSCF to CD-CASPT2. The FNO values depicted refer to the percentage of the trace of the reduced density matrix retained for each case being directly related to the percentage of the total dynamic correlation preserved in the procedure, Figure 2(c and d) provide the total number and the fraction of secondary orbitals frozen in the perturbation step, respectively. As can be seen, the $n_O\pi^*$ state appears to be relatively insensitive to the addition of dynamic correlation by providing similar estimates throughout the full correlation range, yielding small stabilizations with differences between CASSCF and CD-CASPT2 energies of only ∼0.5 eV, in accordance with previous studies that emphasize the relatively secondary role dynamic correlation holds for describing covalent states.[103−105] The amount of correlation included in the different FNO approaches relates well with either the CASSCF or CD-CASPT2 solutions, depending on whether a large or small portion of the secondary space has been trimmed from the perturbation step, respectively. The results depicted in Figure 2(a) stress the unimportant role of dynamic correlation though a variety of FNO approaches, yielding very similar estimates to the CASSCF solution while retaining up to ∼50% of the correlation energy and yielding results within a tenth of an eV of the CD-CASPT2 result while preserving over 90% of the correlation. The $n_O\pi^*$ state is relatively insensitive to the diffuseness of the basis set employed, yielding very similar estimates for 6-31G* as those observed for the larger ANO-L 432/21 basis set, the latter yielding an excited-state order inversion between the $n_O\pi^*$ and $\pi\pi^*$ states that has also been thoroughly discussed, especially for thymine, and that continues to be a topic under debate.[87,88,106,107] Larger deviations can be observed for the ionic $\pi\pi^*$ state, which becomes massively stabilized by over 1.5 eV from the CASSCF to the CD-CASPT2 solution, stressing its dependence on dynamic correlation for its proper description. In this case, the percentage of dynamic correlation retained in the FNO procedure proves crucial to provide accurate estimates by introducing noticeable improvements even when small fractions of the correlation energy (∼20−30%) are included, yielding already shifted results with respect to the CASSCF estimate. A sizable fraction of the secondary orbital space has to be retained in the FNO procedure to present estimates quantitatively analogous to those obtained at the CD-CASPT2 level, emphasizing the importance of the dynamic correlation and setting the threshold of the FNO at ∼95−97.5% to reproduce the CD-CASPT2 data within 0.1 eV. The $\pi\pi^*$ state presents a pronounced dependence on the basis set, being prominently stabilized for the diffuse ANO-L 432/21 while providing similar results for the ANO-L 321/21 and 6-31G* basis sets with differences between the two of ∼0.3 eV, giving rise to the excited-state order inversion previously discussed. In general, the results obtained here with the CD-CASPT2 and highly correlated FNO-CASPT2 schemes are

DOI: 10.1021/acs.jctc.5b00479
J. Chem. Theory Comput. 2015, 11, 3772−3784

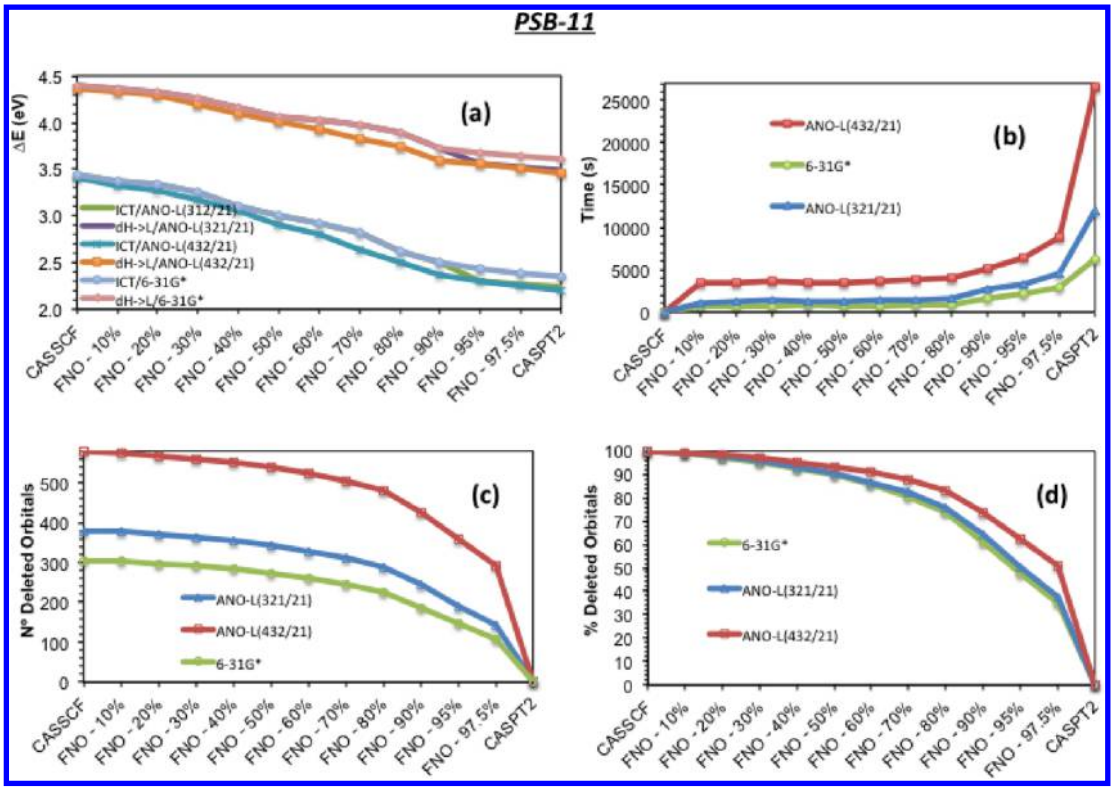

Figure 3. FNO-CASPT2 vs CD-CASPT2 benchmark for PSB-11: (a) vertical excitation energies (ΔE, in eV) for the different FNO schemes and the lowest-lying $\pi\pi^*$ excited states, (b) timings (in s) for the computation of the lowest-lying 3 states of the diverse FNO-CASPT2 calculations with respect to the CD-CASPT2 computation (see text), (c) number of secondary orbitals deleted in the perturbation step, and (d) percentage of the total secondary space deleted in each calculation.

~4.8 and ~4.9 eV for the $\pi\pi^*$ and $n\pi^*$ states, respectively, featuring a different state ordering than those obtained with more correlated single-refence EOMEE-CCSD(T) methods, which yield excitation energies of 4.85 and 5.15 eV.[108] The results obtained here are still within 0.2 eV of the high-level computations available in the literature, highlighting the lower degree of precision of the CASPT2 method compared to complex EOM-CCSD(T) procedures, yet providing a qualitative description of the system. Whereas the state ordering might be somewhat different, it has been shown to be dependent on a variety of factors with the basis set among them; thus, no final statement can be made in this regard, where future experimental evidence may provide an answer.

Figure 2(b) depicts the time required to carry out the second-order perturbation treatment in the different FNO- and CD-CASPT2 schemes. A value of 0 has been given to the CASSCF as it does not feature a subsequent perturbation step. The first evident aspect observed is the dependence of the CD-CASPT2 method on the number of basis set functions included (i.e., the size of the basis set) by increasing the computation time on a 5× factor by going from ANO-L 321/21 to the more diffuse ANO-L 432/21. Both ANO-L 321/21 and 6-31G* basis sets perform analogously, yielding slight differences considered to be negligible. As can be seen, the computational speed-ups relative to the FNO procedure are stalled in the range between 10 and 80%, which points toward a bottleneck related to the set amplitudes arising in CD-CASPT2 from the O inactive + active orbitals as mentioned above, which are not removed in the present procedure. Especially intriguing are the results for the FNO-95% and FNO-97.5% procedures, which present estimates comparable to those of the CD-CASPT2 method but at a lower computational cost. FNO-95% gives rise to computational speed-ups of 2.6× and 3.1× for the ANO-L 321/21 and ANO-L 432/21 basis sets, respectively, whereas FNO-97.5% provides an enhanced 1.8× and 2.1× acceleration, respectively. Panels c and d in Figure 2 provide the number of deleted orbitals and the total percentage of deleted orbitals in the secondary space for the different basis sets. It can be clearly seen that the amount of orbitals deleted to preserve a certain amount of correlations increases dramatically with the size of the basis set, yielding larger speed-ups for the more diffuse basis sets. This becomes particularly apparent when preserving a larger percentage of the trace of the reduced density matrix in the procedure (i.e., FNO-97.5%) by yielding a difference of up to 10% between the total deleted orbitals in the procedure for the ANO-L 432/21 and ANO-L 321/21 basis sets, highlighting the increasing computational gains with basis set size, thus allowing the use of larger basis sets to obtain more converged vertical excitation energies within an ab initio approach.

PSB-11 has been considered next as it features a larger molecular frame in which all of the speed-ups previously described will be pronouncedly outstretched and assessed. It contains 52 atoms, as opposed to the 15 featured by thymine, implying a larger number of basis set functions to be spanned within a certain basis set. Two types of excited-state transitions have been analyzed: the $\pi\pi^*$ intramolecular charge transfer (ICT) state and the doubly excited $\pi\pi^*$ HOMO to LUMO transition (dH → L). The former presents a very pronounced ionic character, whereas the latter can be considered to be more covalent in comparison, therefore pointing toward a similar scenario as that laid out for thymine in which dynamic correlation affects the diverse excited states featured in the

DOI: 10.1021/acs.jctc.5b00479
J. Chem. Theory Comput. 2015, 11, 3772−3784

Table 1. Main Geometrical Optimized Parameters for the Ground- and First-Excited State at the CASSCF, CD-CASPT2, FNO-97.5%, and FNO-95% Levels of Theory for PSB-3[a]

	C_9-C_5	C_5-C_2	C_2-C_1	C_1-C_3	C_3-N	RMSD wrt CD-CASPT2
				S_0		
CD−CASPT2	1.3560	1.4381	1.3758	1.4137	1.3139	
CASSCF	1.3482	1.4416	1.3700	1.4181	1.2933	0.02346
FNO−95%	1.3377	1.4553	1.3708	1.4252	1.3098	0.02837
FNO−97.5%	1.3504	1.4387	1.3769	1.4120	1.3122	0.00622
				S_1		
CD−CASPT2	1.3882	1.4270	1.4308	1.4244	1.3526	
$CASSCF_{bi}$	1.4086	1.3728	1.5219	1.3784	1.3561	0.12452
$CASSCF_{no-bi}$	1.3878	1.4221	1.4308	1.4244	1.3526	0.01111
FNO−95%	1.3843	1.4325	1.4209	1.4365	1.3602	0.01036
FNO−97.5%	1.3849	1.4278	1.4240	1.4320	1.3576	0.00408

[a]Atomic labeling refers to those described in Figure 1. All calculations have been carried out making use of the 6-31G* basis set. All distances are given in Å.

photoprocess differently. Figure 3 presents the vertical excitation energies for a range of FNO schemes between the CASSCF and CD-CASPT2 solutions. As can be seen, the addition of dynamic correlation is in this case much more pronounced than those observed in thymine, as the two excited states featured in PSB-11 present a profound dependence of dynamic correlation given their ionic character. The lowest-lying and spectroscopic ICT state becomes stabilized by ∼1.5 eV by going from the CASSCF to the CD-CASPT2 results, whereas the dH → L state presents a somewhat lower stabilization of ∼1 eV, being still pronounced compared to the results obtained for a fully covalent state as discussed above. A plateau seems to be reached by including ≥90% of the correlation energy for both excited states, providing accurate descriptions within ∼0.15 eV of the CD-CASPT2 result. The basis set effect is in this case less pronounced, yielding vertical excitation energies within 0.2 eV for all basis sets and along the whole correlation range analyzed. Figure 3(b) shows the relative computational speed-ups for the different FNO schemes and the diverse basis sets employed. As can be seen, a similar plateau can be recognized as in the case of thymine, where for the FNO, 10−80% range no speed-ups are observed as they arise from the *O* inactive + active set of orbitals. This means that no additional speed-up is gained by lowering the FNO procedure under the 80% threshold, thus discouraging any computation under this mark. Large computational savings can be noticed for the largest ANO-L 432/21 basis set, whereas pronounced accelerations are still observed for the smaller ANO-L 321/21 and 6-31G* basis sets that again perform analogously. For the more correlated FNO-95% and FNO-97.5%, more pronounced speed-ups can be readily seen, yielding over a 4-fold acceleration for the former and 3-fold for the latter by employing the larger ANO-L 432/21 basis set, and a 3× and 2.2× for the smaller ANO-L 321/21, respectively. Panels c and d in Figure 3 depict the orbitals kept frozen along the perturbation step for the different FNO schemes studied. Similar conclusions can be drawn as those previously discussed for thymine, being more pronounced, highlighting the role the number of basis set functions spanned plays on the acceleration of the FNO approach where close to 60% of the secondary orbitals are deleted for the more correlated FNO-97.5% procedure.

In terms of dynamic correlation to be retained in the FNO procedure, it has been shown that it is strongly dependent on the nature of the state under study. Even though covalent states require a lesser amount of dynamic correlation to be properly described, ionic states still present a challenge in this respect by being highly dependent on the correlation included in the procedure. As the final goal of the newly introduced method is to be employed for elucidating photoinduced phenomena, an accurate description of a variety of excited states of different nature on an equal footing is of paramount importance. With this in mind and on the basis of the results obtained for the two biologically relevant systems analyzed here, a threshold value of ∼95−97.5% is advised here to tackle vertical excitation energies within an FNO-CASPT2 approach, yielding up to 4-fold speed-ups while providing essentially equivalent results as those obtained within the CD-CASPT2 method.

3.2. Geometry Optimizations: a CD-CASPT2//FNO-CASPT2 Protocol. Even though the first implementation of the analytical fully internally contracted CASPT2 gradients has been recently introduced,[109] the numerical nature of the CD-CASPT2 and FNO-CASPT2 implementations currently available to us hampers the study of large molecules due to computational demands. With this in mind, two different systems of moderate size, PSB-3 and thymine, have been analyzed by considering their main optimized geometrical parameters in their ground and electronic excited states as a benchmark for gradient computations. CASPT2 geometry optimizations are not routinely employed due to the high computational cost associated,[110,111] as well as due to the lack, until very recently,[109] of analytical gradients that were only available for its uncontracted formulation, which proves too expensive for routine applications with moderate active spaces.[41,47] The approach commonly taken in theoretical photochemical studies is based on performing the gradient computations and thus the mapping of the potential energy hypersurfaces at the cheaper CASSCF level. This assumption considers that this method is accurate enough to describe the geometrical deformations occurring in the system while a correction on the key structures so obtained is performed by computing their energy at the CASPT2 level in what is widely known as the CASPT2//CASSCF protocol. This protocol has been successfully employed over the last two decades to provide a molecular counterpart to a plethora of spectroscopic experimental data, elucidating the concrete decay channels and photoinduced mechanisms in a wide range of biomolecular systems.[88,112]

Nevertheless, the assumption taken on the correct description of CASSCF geometries has to be handled with care, as depending on the molecular system under study and the specific inter- and intramolecular interactions displayed, this might

DOI: 10.1021/acs.jctc.5b00479
J. Chem. Theory Comput. 2015, 11, 3772−3784

prove to not be as straightforward as commonly thought.[113−117] For this very reason, a computationally efficient CASPT2 approach that allows mapping of the ground- and excited-state potential energy hypersurfaces is of paramount interest. The new implementation of the FNO-CASPT2 method has been developed with this in mind, as it yields analogous results to that of its CD-CASPT2 counterpart for a variety of nuclear arrangements while providing large speed-ups that make numerical gradient computations feasible. A proper characterization of the potential energy hypersurfaces of biological chromophores of interest within multiconfigurational dynamically correlated methods seems timely and holds the premise to solve many of the present difficulties faced by the methods currently employed based mainly on CASSCF gradients, such as those arisen in molecular dynamics and optimization/minimum energy path calculations due to the wrong energetic order of the excited state manifold at the CASSCF level or to an inadequate description of the potential energy hypersurface manifested by the lack of dynamic correlation.

The main geometrical optimized parameters of PSB-3 are given in Table 1 and Figure 4. As can be seen, two different

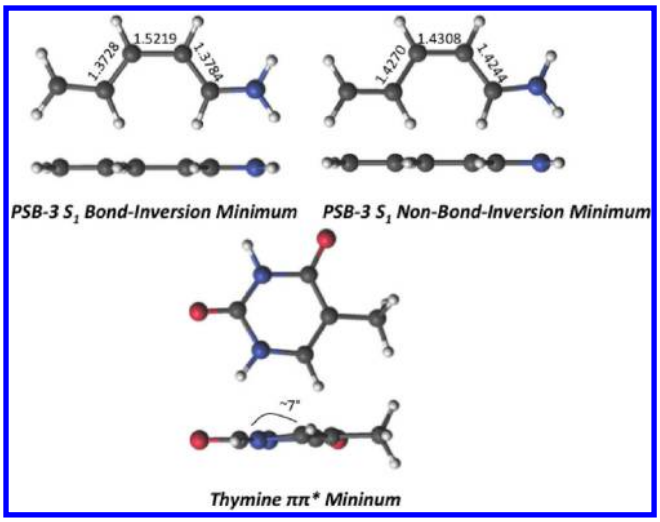

Figure 4. Excited state minima characterized for PSB-3 and thymine together with their main structural distortions.

FNO schemes (95% and 97.5%) have been employed and compared to the CASSCF and CD-CASPT2 results. Both FNO procedures perform relatively well with respect to the CD-CASPT2 reference, yielding ∼2 pm deviations for the less- and sub-pm distortions for the most-correlated scenario. The values obtained here are also in agreement with those provided at the CASPT2 and quantum Monte Carlo levels of theory,[113] pointing toward non-negligible differences between the correlated and uncorrelated CASSCF geometries. These differences are stressed when optimizing the S_1 excited state, yielding different qualitative results. At the CASSCF level of theory, two different minima are characterized along the S_1 potential energy hypersurface,[84] (i) a bond inversion minimum (coined $CASSCF_{bi}$) where a partial charge-transfer event is already taking place, thus prompting the system toward its photoisomerization, and (ii) a minimum where no bond inversion can be observed (coined $CASSCF_{no-bi}$) and that prevents photoisomerization. The former is shown to be more stable at the CASSCF level of theory, whereas the latter appears to be the only solution found within multireference correlated methods reported in the literature as well as in all different FNO and CD-CASPT2 results shown here.[113] Whereas the average root-mean-square deviations over all bond lengths might be relatively small, the effects of these two different outcomes prominently affect the conclusions drawn for the photochemical pathways followed by the system. Within a CASSCF approach, the system will photoisomerize in an ultrafast manner,[84] whereas at the CASPT2 level, the no-bond inversion minimum prevails, preventing isomerization as the system would have to surmount a minimum barrier of ∼0.2 eV at the CD-CASPT2 level to access the bond-inversion structure that propels the photoisomerization. This points toward a hampering of the photoisomerization event at the higher level of theory, contrary to what has been observed over the years through experimental evidence. Nevertheless, these systems are also profoundly dependent on the solvent and the proteic environment where they are embedded, which are also the conditions in which the experiments are normally conducted.[86] The polar environment where the system is embedded is likely to stabilize the highly polar $\pi\pi^*$ intramolecular charge transfer state, thus reducing the barrier present between the bond- and nonbond-inversion minima and therefore enhancing the photoisomerization event.[118] Modifications of the proteic medium, and specifically of the pocket where the chromophore is embedded, as well as the nature of the chromophore, can also drastically affect the isomerization rate, as has recently been shown.[119] It can therefore be concluded that the proper characterization of the photoinduced pathways on biochromophores might be dependent on several factors with the usage of dynamically correlated methods in the hypersurface mapping being one of them. This highlights the importance of introducing cost-efficient computational protocols that allow for improving the estimates yielded by CASSCF-like approaches over the last two decades while pointing toward the erroneous behavior given within this approach in cases where dynamic correlation is prominent, as is usually the case in systems governed by intermolecular interactions.[114,120]

Thymine was studied next as it provides a very interesting case on the role dynamic correlation plays in the mapping of potential energy hypersurfaces in the excited state. Thymine is one of the canonical DNA nucleobases, the main chromophoric components of the genetic code, and presents the longest lifetime registered for monomeric species.[88,106,121] Its concrete photoinduced dynamics are still under heated debate, as several explanations to rationalize the experimental kinetic time scales have been put forth, yielding a variety of different mechanisms depending on the approach and method employed. Thymine has two experimentally defined decay constants:[122] one ultrafast of ∼100 fs that is widely attributed to a barrierless decay toward an ethene-like conical intersection with the ground state of the initially accessed bright $\pi\pi^*$ state,[87,88] or to the population transfer between the initially accessed bright $S_2-\pi\pi^*$ state and the lower-lying $n_O\pi^*$ state,[107] whereas the longer lived ∼5.2 ps signal is usually attributed to the presence of a minimum in a region of the $\pi\pi^*$ state hypersurface[87,123,124] that traps the population, increasing its lifetime, or even to deactivation through the nonadiabatically accessed $n_O\pi^*$ state.[125] The aforementioned minimum of the $\pi\pi^*$ state has also been suggested to be placed either before the crossing with the $n_O\pi^*$ state[123] or after the crossing once the $\pi\pi^*$ state becomes S_1 on the way toward the ethene-like conical intersection with the ground state.[107,124]

DOI: 10.1021/acs.jctc.5b00479
J. Chem. Theory Comput. 2015, 11, 3772−3784

As can be seen, the specific mechanism accounting for the different time scales remains under heated debate,[106] even more so for the photoinduced pathways present in vacuo, whereas recent works have shed light on the events occurring in solution,[126] where the blue-shift suffered by the $n_O\pi^*$ state is expected to hamper its involvement in the photoprocess.[126−128] In the gas phase, thymine presents very close $\pi\pi^*$ and $n_O\pi^*$ excited states that are likely to interact in the vicinities of the Franck−Condon region.[129−131] This points toward an ultrafast population transfer between the initially accessed bright $\pi\pi^*$ state and the $n_O\pi^*$ state, the latter being lower or higher in energy than the former depending on the basis set employed, as has been shown above. These excited states are of very different natures, the former being strongly ionic and the latter being pronouncedly covalent, as has been discussed at length previously in the benchmark of their vertical excitation energies. The energetic differences between the two states range between ∼0.2 eV at the CASPT2,[87,88] CD-CASPT2, or FNO-CASPT2 levels of theory, facilitating the nonadiabatic interaction, whereas a more pronounced difference of ∼1.5 eV is given at the CASSCF level. At this level, a higher lying $n_o\pi^*$ state at approximately the same energy region as the $\pi\pi^*$ state appears, which gives rise to an artificial interaction due to the overestimated energetic position of the $\pi\pi^*$ state affecting its photoinduced decay, shedding some doubts on the applicability of the CASSCF method for this particular problem.[129] The method employed to characterize these states and to explore their potential energy hypersurfaces is therefore bound to profoundly influence the fate of the calculation and subsequently shape its interpretation of the available experimental data, as the larger initial difference in energy yielded at the CASSCF could very well account for the first ∼100 fs time constant related to reaching the intersection between $\pi\pi^*$ and $n_O\pi^*$. The smaller energy gap and the lower-lying position at the CASPT2 level of theory of the $\pi\pi^*$ state, on the other hand, may point toward a different scenario, highlighting the diverse conclusions that may be reached depending on the level of theory employed and emphasizing the development and usage of more correlated approaches to map the excited-state hypersurface in static and dynamic photoinduced mechanistic studies of biochromophores.

Table 2 displays the different bond lengths obtained at the CASSCF, CD-CASPT2, and FNO-CASPT2 levels of theory for thymine in its ground- and lowest-lying $\pi\pi^*$ excited state. As can be seen, small deviations in their bond length distances are given for the electronic ground state, as was the case in PSB-3, whereas large differences are yielded for the $\pi\pi^*$ state when comparing the diverse CASPT2 protocols with the CASSCF results. This is due to the different outcomes of the optimizations at the CASSCF and CASPT2 levels of theory, the former yielding a barrierless decay ending in the ethene-like conical intersection along its minimum energy path.[87] Table 2 refers the CASSCF distances to this ethene-like CI, thus yielding large discrepancies, whereas the CASPT2 results show a slightly distorted (∼7° in the dihedral responsible for the pyramidalization motion, see Figure 4) ring-puckering minimum that prevents its evolution toward the crossing.[124] This difference in the qualitative behavior of the methods stresses the importance of employing more accurate techniques to compute the gradients to map the hypersurfaces explored in theoretical photochemical studies, as the different solutions yielded might suggest completely different photochemical scenarios and a distinct interpretation of the experimental evidence. It must also be stressed that the energy barrier to be surmounted by this minimum at the CASPT2 level of theory has been reported to be around a tenth of an eV,[124] yielding a complex scenario in which no clear statement can be made regarding the fate of the photochemical reaction, as both an ultrafast decay[87] and a population trap in this minimum[123] could be supported. Providing a conclusive answer would require high-level nonadiabatic molecular dynamics to be employed[123,125] coupled with highly correlated electronic structure theory methods as to the ones presented here, as the shape of the potential energy hypersurfaces seems to be dependent on the dynamic correlation lacking at the CASSCF level.

Table 2. Main Geometrical Optimized Parameters for the Ground- and First-Excited State at the CASSCF, CD-CASPT2, FNO-97.5%, and FNO-95% Levels of Theory for Thymine[a]

	CD−CASPT2	CASSCF	FNO−95%	FNO−97.5%
		S_0		
N_1-H_{11}	1.0256	1.0009	1.0241	1.0241
N_1-C_7	1.4114	1.3871	1.4141	1.4088
C_7-O_8	1.2278	1.2011	1.2248	1.2325
C_7-C_5	1.4724	1.4761	1.4752	1.4840
C_5-C_6	1.5047	1.5031	1.5219	1.4989
C_5-C_4	1.3652	1.3456	1.3634	1.3620
C_4-H_{10}	1.0921	1.0768	1.0851	1.0830
C_4-N_2	1.3869	1.3860	1.3803	1.3829
N_2-H_{12}	1.0207	0.9972	1.0210	1.0220
N_2-C_3	1.3918	1.3678	1.3812	1.3837
C_3-O_9	1.2255	1.1981	1.2199	1.2209
C_3-N_1	1.3923	1.3776	1.3995	1.3952
RMSD wrt CD-CASPT2		0.06815	0.02477	0.02013
n° iters	7		14	7
		$\pi\pi^*$		
N_1-H_{11}	1.0010	1.0010	1.0293	1.0248
N_1-C_7	1.4584	1.4257	1.4689	1.4750
C_7-O_8	1.2623	1.2432	1.2577	1.2733
C_7-C_5	1.4342	1.3867	1.4398	1.4441
C_5-C_6	1.4988	1.5004	1.4944	1.4819
C_5-C_4	1.4552	1.5232	1.4546	1.4609
C_4-H_{10}	1.0907	1.0735	1.0846	1.0893
C_4-N_2	1.3780	1.3326	1.3645	1.3741
N_2-H_{12}	1.0298	1.0070	1.0274	1.0324
N_2-C_3	1.4382	1.4142	1.4168	1.4297
C_3-O_9	1.2344	1.2017	1.2315	1.2282
C_3-N_1	1.3608	1.3414	1.3685	1.3573
RMSD wrt CD-CASPT2		0.11740	0.03088	0.03098
n° iters	19		30	18

[a]Atomic labeling refers to those described in Figure 1. All calculations have been carried out making use of the 6-31G* basis set. CASSCF structures have been taken from ref 87 (see text for further details). All distances are given in Å.

By close inspection of Table 2, it can be seen that both FNO procedures presented, FNO-95% and FNO-97.5%, yield accurate results within 3 pm of the ones obtained at the CD-CASPT2 level. The gradients obtained with these methods show strong similarities and are therefore expected to yield qualitatively analogous results, even though some numerical instability appears in the less correlated FNO-95%. This can be observed by comparing the number of iterations required to

DOI: 10.1021/acs.jctc.5b00479
J. Chem. Theory Comput. 2015, 11, 3772−3784

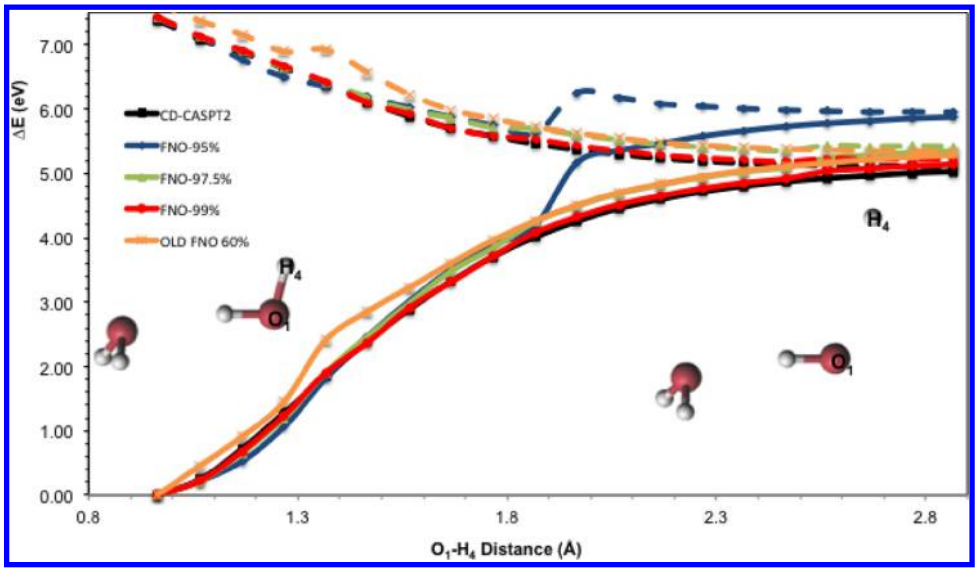

Figure 5. CASPT2(16,12)/ANO-L O[5s4p1d]/H[2s1p] potential energy curves describing the photodissociation of the water dimer with respect to the intramolecular O_1-H_4 distance.[90] Dashed lines represent the lowest-lying S_1-$\pi\sigma^*$ electronic excited state energies, whereas full lines refer to the ground state. The geometries of the water dimer at the Franck−Condon region (left-hand side) and at the dissociation limit (right-hand side) have also been given to provide a visual aid of the photoprocess.

reach the minimum, requiring twice as many points for the ground state and ∼66% more structures at the $\pi\pi^*$ excited state to reach the same result. Conversely, the more correlated FNO-97.5% performs much better, requiring roughly the same number of steps as its CD-CASPT2 counterpart. This might be due to the numerical nature of the gradient computation, but it highlights the importance of the single-point accuracy to yield precise gradients, preferring the more expensive FNO-97.5% over the FNO-95% procedure because it will require less optimization steps and will therefore be faster computationally. This conclusion can be extended to any static optimization/minimum energy path scheme as well as in time-dependent molecular dynamics simulations given that the more correlated approach will yield more accurate gradients with lower numerical instabilities, avoiding as much as possible the numerical noise introduced along the trajectory.

3.3. Dissociation Curves. The last test case to ensure the reliability of our new implementation of the FNO scheme examines the description of the photodissociation process triggered in the water dimer upon UV-light absorption.[90] Dissociation processes require a multiconfigurational treatment for its proper portrayal, as the wave function smoothly changes its character along the pathway toward the dissociation limit where the species separates into two moieties. A large number of photochemical events occurring in biomolecules have been accredited to photodissociation processes mainly based on dark $\pi\sigma^*$ states. These states become populated in the vicinities of the Franck−Condon region due to its close-lying energetic position with the spectroscopic states, propelling a bond stretching motion that ends up in dissociation events.[132−136] Such processes are therefore expected to be ubiquitous in nature, and their correct description is of paramount importance to elucidate the photoinduced mechanisms governing UV-irradiated biochromophores and related molecules of interest. Its importance can also be extended to dimeric and multimeric systems, especially those governed by strong intermolecular interactions (i.e., π-stacking interactions), where the mulficonfigurational nature of the excited state described is expected to change along the intermolecular distance. In fact, one often goes from a delocalized (or excitonic) state at short distances to excited states localized in the diverse moieties at longer range, thus requiring a solid method to account for the smooth changes in energy registered along the intermolecular distance.[137,138]

In the test case provided here, the S_1-$\pi\sigma^*$ state in the water dimer is localized in the water donor molecule (i.e., the water moiety that *donates* a hydrogen bond in the right-hand side on the molecular structure provided in Figure 1, referring to the other moiety as the water *acceptor*),[90] prompting an elongation along the O_1-H_4 distance associated with the σ^* antibonding orbital characterizing the electronic transition. Extensive minimum energy path and molecular dynamics calculations previously reported in ref 90 show that the main reaction coordinate is the O_1-H_4 bond elongation with negligible contributions from other degrees of freedom, thus allowing the construction of the PES solely based on this bond stretching motion. Figure 5 displays the potential energy curves resulting at different levels of theory, namely, CD-CASPT2, FNO-95%, FNO-97.5%, and FNO-99%. The first electronic excited state (S_1-$\pi\sigma^*$) is represented with dashed lines, whereas the ground state is depicted with full lines, and the two states meet at the dissociation limit that is placed at ∼5.1 eV adiabatically from the Franck−Condon region at the reference CD-CASPT2 level, in agreement with previous estimates employing the standard CASPT2 technique.[90] A quick inspection of Figure 5 shows a smooth decay in energy of the first excited state and a progressive increase in energy of the ground state leading to a crossing between the two states at the dissociation limit. As can be seen in Figure 5, the smooth evolution of the energy with respect to the O_1-H_4 distance is provided by the more correlated approaches, CD-CASPT2 (black), FNO-97.5% (green), and FNO-99% (red), whereas FNO-95% (blue) breaks down at ∼1.8 Å distance, yielding an unphysical barrier along the pathway that results in a wrong estimate of the dissociation limit, being placed at ∼5.9 eV, nearly 1 eV higher in energy with respect to the CD-CASPT2 reference. It must be noted that the vertical excitation energies at the Franck−Condon region and its vicinities are equally well described at all levels of theory employed, resulting in vertical excitation energies of ∼7.36 eV,[90]

DOI: 10.1021/acs.jctc.5b00479
J. Chem. Theory Comput. 2015, 11, 3772−3784

in agreement with the 7.37 eV obtained with more accurate CR-EOMCCSD(T)/6-311(2+)G* methods,[139] with the problems arising at longer O_1-H_4 distances along the photodissociation process. Similar difficulties at a smaller degree are found by employing an FNO-97.5% scheme, yielding a much less pronounced barrier at distances of ∼2.6 Å, leading again to an overestimation of the energy at the dissociation limit being placed at ∼5.4 eV, ∼0.3 eV higher than the reference. These problems can be fixed by increasing the correlation in the calculation, as can be seen by the behavior of the FNO-95% and FNO-97.5% schemes, and especially by employing a more correlated FNO-99%, which features a barrierless decay path that is in agreement with the reference CD-CASPT2 result and being placed within a tenth of an eV of the dissociation limit. Additionally, results arising from the old implementation of the FNO-CASPT2 employing 60% of the virtual space in the correlation step have been added, as to highlight the abrupt behavior presented along the potential energy surface and stressing the motivation of the present work. It is also worth noting that 60% of the virtual space relates with the amount of virtual orbitals included in the different FNO schemes depicted in Figure 5, which in this case are selected by means of the trace of the approximate reduced density matrix instead, such that all results depicted are indeed comparable.

Photodissociation processes are therefore expected to be extremely difficult to represent by making use of truncated schemes, such as the one presented here. Nevertheless, it has been shown that the newly implemented FNO is capable of CD-CASPT2 performance if enough correlation energy is included, requiring a larger amount of correlation in this case than in any other property previously analyzed. It is worth noting that even though 99% of the correlation energy had to be retained for the method to be applicable for these intricate and difficult photodissociation processes, a remarkable speed-up is still attained as 1% of the approximate trace of the reduced density matrix translates in the truncation of ∼32% of the total virtual space, which is expected to be even bigger for larger and more diffuse basis sets as well as for larger molecular systems. The degree of accuracy attained also points toward its possible application to map potential energy surfaces of both ground and excited electronic states with more accurate techniques that would become feasible due to the sizable speed-ups provided in this new implementation.[140]

4. SUMMARY

With the advent of Cholesky decomposition (CD) techniques, multiconfigurational perturbation theory in the form of CASSCF/CASPT2 calculations have gradually moved from the study of small model systems to a tool that can provide accurate results in the investigation of the most general chemical processes. In particular, one can achieve substantial reduction in computational costs by operating a truncation of the virtual space that systematically introduces hierarchical contributions to the correlation energy. This approach of freezing some (approximate) natural orbitals from the perturbative correction, widely employed for many-body perturbation theory single reference methods, has been extended to multiconfigurational second-order perturbation theory (FNO-CASPT2) and allows for moving the application limit of CD-CASPT2 to much larger molecules and very accurate basis sets.

The present paper calls attention to the problems encountered when attempting to use the benefits of FNO-CASPT2 in photochemical studies. By nature, the latter require approximations that are uniformly accurate along potential energy surfaces and that provide sufficiently accurate forces in molecular dynamics studies. To overcome such problems, we have proposed a new implementation of FNO-CASPT2 where we truncate the virtual space by excluding those orbitals that contribute the least toward preserving a predefined value of the trace of the approximate density matrix used to define the NOs. This quantity is proportional to the amount of correlation retained in the procedure and can be used to guarantee that the amount of correlation included is preserved at all nuclear arrangements.

The importance of mapping the potential energy surfaces within a multiconfigurational dynamically correlated approach cannot be overstated, and a few biochromophoric species are given as examples, including the nucleobase thymine in particular, where different excited-state behaviors can be discerned depending on the CASSCF or CASPT2 mapping of the surfaces, which is bound to profoundly influence the molecular interpretation of the available experimental evidence. This calls attention to the general applicability of the routinely employed CASPT2//CASSCF protocol and proposes more correlated approaches for those cases where CASSCF does not yield a proper description of the electronic structure, mainly in systems governed by strong intermolecular interactions or with close-lying excited-states featuring very different natures with a highly unbalanced dependence on the dynamical correlation.

The approach has been benchmarked and shown to lead to massive speed-ups while retaining the accuracy achieved in CD-CASPT2 computations with errors within a tenth of an eV for excitation energies and absolutely negligible in gradients calculations. It is therefore perfectly sensible to believe that future multiconfigurational wave function theory studies in photochemistry and other areas will make extensive use of this approach to make more and more realistic simulations affordable at a high level of accuracy.

AUTHOR INFORMATION

Corresponding Authors

*E-mail: javier.segarra@unibo.it.
*E-mail: marco.garavelli@unibo.it, marco.garavelli@ens-lyon.fr.
*E-mail: francesco.aquilante@gmail.com.

Notes

The authors declare no competing financial interest.

ACKNOWLEDGMENTS

M.G. acknowledges support by the European Research Council Advanced Grant STRATUS (ERC-2011-AdG No. 291198). F.A. gratefully acknowledges support from the FIRB "PROGRAMMA FUTURO IN RICERCA" RBFR1248UI from the Italian government. The authors wish to thank the reviewers for providing constructive feedback that vastly improved the manuscript.

REFERENCES

(1) Roos, B. O.; Taylor, P. R.; Sigbahn, P. E. *Chem. Phys.* **1980**, *48*, 157−173.
(2) Olsen, J.; Roos, B. O.; Jörgensen, P.; Jensen, H. J. *J. Chem. Phys.* **1988**, *89*, 2185.
(3) Knowles, P. J.; Werner, H.-J. *Chem. Phys. Lett.* **1985**, *115*, 259−267.
(4) Werner, H.-J.; Knowles, P. J. *J. Chem. Phys.* **1985**, *82*, 5053.
(5) Szalay, P. G.; Müller, T.; Gidofalvi, G.; Lischka, H.; Shepard, R. *Chem. Rev.* **2012**, *112*, 108−181.

DOI: 10.1021/acs.jctc.5b00479
J. Chem. Theory Comput. 2015, 11, 3772−3784

(6) Ruedenberg, K.; Schmidt, M. W.; Gilbert, M. M.; Elbert, S. T. *Chem. Phys.* **1982**, *71*, 41−49.
(7) Serrano-Andrés, L.; Merchán, M. *J. Mol. Struct.: THEOCHEM* **2005**, *729*, 99−108.
(8) González, L.; Escudero, D.; Serrano-Andrés, L. *ChemPhysChem* **2012**, *13*, 28−51.
(9) Roos, B. O. *Adv. Chem. Phys.* **1987**, *69*, 399−446.
(10) Meier, U.; Staemmler, V. *Theor. Chim. Acta* **1989**, *76*, 95−111.
(11) Veryazov, V.; Malmqvist, P. Å; Roos, B. O. *Int. J. Quantum Chem.* **2011**, *111*, 3329−3338.
(12) White, S. R. *Phys. Rev. Lett.* **1992**, *69*, 2863−2866.
(13) Chan, G. K. L.; Sharma, S. *Annu. Rev. Phys. Chem.* **2011**, *62*, 465−481.
(14) Yanai, T.; Kurashige, Y.; Neuscamman, E.; Chan, G. K. L. *J. Chem. Phys.* **2010**, *132*, 024105.
(15) Shepard, R.; Gidofalvi, G.; Brozell, S. R. *J. Chem. Phys.* **2014**, *141*, 064105.
(16) Shepard, R.; Gidofalvi, G.; Brozell, S. R. *J. Chem. Phys.* **2014**, *141*, 064106.
(17) Szabo, A.; Ostlund, N. S. *Modern Quantum Chemistry*; Dover, 1996.
(18) Manni, G. L.; Aquilante, F.; Gagliardi, L. *J. Chem. Phys.* **2011**, *134*, 034114.
(19) Li Manni, G.; Ma, D.; Aquilante, F.; Olsen, J.; Gagliardi, L. *J. Chem. Theory Comput.* **2013**, *9*, 3375−3384.
(20) Malrieu, J.-P.; Heully, J.-L.; Zaitsevskii, A. *Theor. Chim. Acta* **1995**, *90*, 167−187.
(21) Andersson, K.; Malmqvist, P.-Å; Roos, B. O. *J. Chem. Phys.* **1992**, *96*, 1218−1226.
(22) Roca-Sanjuán, D.; Aquilante, F.; Lindh, R. *WIRES Comput. Mol. Sci.* **2012**, *2*, 585−603.
(23) Angeli, C.; Pastore, M.; Cimiraglia, R. *Theor. Chem. Acc.* **2007**, *117*, 743−754.
(24) Celani, P.; Werner, H.-J. *J. Chem. Phys.* **2000**, *112*, 5546.
(25) Kurashige, Y.; Chalupsky, J.; Lan, T. N.; Yanai, T. *J. Chem. Phys.* **2014**, *141*, 174111.
(26) Sharma, S.; Chan, G. K. L. *J. Chem. Phys.* **2014**, *141*, 111101.
(27) Shiozaki, T.; Werner, H.-J. *J. Chem. Phys.* **2010**, *133*, 141103.
(28) Lyakh, D. I.; Musiał, M.; Lotrich, V. F.; Bartlett, R. J. *Chem. Rev.* **2012**, *112*, 182−243.
(29) Musiał, M.; Perera, A.; Bartlett, R. J. *J. Chem. Phys.* **2011**, *134*, 114108.
(30) Datta, D.; Nooijen, M. *J. Chem. Phys.* **2012**, *137*, 204107.
(31) Samanta, P. K.; Mukherjee, D.; Hanauer, M.; Köhn, A. *J. Chem. Phys.* **2014**, *140*, 134108.
(32) Lischka, H.; Shepard, R.; Brown, F. B.; Shavitt, I. *Int. J. Quantum Chem.* **1981**, *20*, 91−100.
(33) Shiozaki, T.; Knizia, G.; Werner, H.-J. *J. Chem. Phys.* **2011**, *134*, 034113.
(34) Li Manni, G.; Carlson, R. K.; Luo, S.; Ma, D.; Olsen, J.; Truhlar, D. G.; Gagliardi, L. *J. Chem. Theory Comput.* **2014**, *10*, 3669−3680.
(35) Dresselhaus, T.; Neugebauer, J.; Knecht, S.; Keller, S.; Ma, Y.; Reiher, M. *J. Chem. Phys.* **2015**, *142*, 044111.
(36) Yanai, T.; Chan, G. K. L. *J. Chem. Phys.* **2006**, *124*, 194106.
(37) Neuscamman, E.; Yanai, T.; Chan, G. K.-L. *Int. Rev. Phys. Chem.* **2010**, *29*, 231−271.
(38) Andersson, K.; Malmqvist, P. A.; Roos, B. O.; Sadlej, A. J.; Wolinski, K. *J. Phys. Chem.* **1990**, *94*, 5483−5488.
(39) Farahani, P.; Roca-Sanjuán, D.; Aquilante, F. *J. Comput. Chem.* **2014**, *35*, 1609−1617.
(40) Finley, J.; Malmqvist, P.-Å; Roos, B. O.; Serrano-Andrés, L. *Chem. Phys. Lett.* **1998**, *288*, 299−306.
(41) Shiozaki, T.; Györffy, W.; Celani, P.; Werner, H.-J. *J. Chem. Phys.* **2011**, *135*, 081106.
(42) Granovsky, A. A. *J. Chem. Phys.* **2011**, *134*, 214113.
(43) Aquilante, F.; Pedersen, T. B.; Lindh, R.; Roos, B. O.; Sánchez de Merás, A.; Koch, H. *J. Chem. Phys.* **2008**, *129*, 024113.
(44) Boström, J.; Aquilante, F.; Pedersen, T. B.; Lindh, R. *J. Chem. Theory Comput.* **2009**, *5*, 1545−1553.
(45) Aquilante, F.; Malmqvist, P.-Å; Pedersen, T. B.; Ghosh, A.; Roos, B. O. *J. Chem. Theory Comput.* **2008**, *4*, 694−702.
(46) Boström, J.; Delcey, M. G.; Aquilante, F.; Serrano-Andrés, L.; Pedersen, T. B.; Lindh, R. *J. Chem. Theory Comput.* **2010**, *6*, 747−754.
(47) Györffy, W.; Shiozaki, T.; Knizia, G.; Werner, H.-J. *J. Chem. Phys.* **2013**, *138*, 104104.
(48) Aquilante, F.; Todorova, T. K.; Gagliardi, L.; Pedersen, T. B.; Roos, B. O. *J. Chem. Phys.* **2009**, *131*, 034113.
(49) Pulay, P. *Chem. Phys. Lett.* **1983**, *100*, 151−154.
(50) Sæbø, S.; Pulay, P. *Chem. Phys. Lett.* **1985**, *113*, 13−18.
(51) Sæbø, S.; Pulay, P. *J. Chem. Phys.* **1988**, *88*, 1884.
(52) Meyer, W. *J. Chem. Phys.* **1973**, *58*, 1017.
(53) Ahlrichs, R.; Driessler, F.; Lischka, H.; Staemmler, V.; Kutzelnigg, W. *J. Chem. Phys.* **1975**, *62*, 1235.
(54) Löwdin, P.-O. *Phys. Rev.* **1955**, *97*, 1474−1489.
(55) Hättig, C.; Tew, D. P.; Helmich, B. *J. Chem. Phys.* **2012**, *136*, 204105.
(56) Hättig, C.; Klopper, W.; Köhn, A.; Tew, D. P. *Chem. Rev.* **2012**, *112*, 4−74.
(57) Hetzer, G.; Schütz, M.; Stoll, H.; Werner, H.-J. *J. Chem. Phys.* **2000**, *113*, 9443.
(58) Kats, D. *J. Chem. Phys.* **2014**, *141*, 244101.
(59) Köppl, C.; Werner, H.-J. *J. Chem. Phys.* **2015**, *142*, 164108.
(60) Krause, C.; Werner, H.-J. *Phys. Chem. Chem. Phys.* **2012**, *14*, 7591−7604.
(61) Neese, F.; Wennmohs, F.; Hansen, A. *J. Chem. Phys.* **2009**, *130*, 114108.
(62) Hansen, A.; Liakos, D. G.; Neese, F. *J. Chem. Phys.* **2011**, *135*, 214102.
(63) Riplinger, C.; Neese, F. *J. Chem. Phys.* **2013**, *138*, 034106.
(64) Liakos, D. G.; Sparta, M.; Kesharwani, M. K.; Martin, J. M. L.; Neese, F. *J. Chem. Theory Comput.* **2015**, *11*, 1525−1539.
(65) Schwilk, M.; Usvyat, D.; Werner, H.-J. *J. Chem. Phys.* **2015**, *142*, 121102.
(66) Werner, H.-J.; Knizia, G.; Krause, C.; Schwilk, M.; Dornbach, M. *J. Chem. Theory Comput.* **2015**, *11*, 484−507.
(67) Manby, F. R.; Werner, H.-J.; Adler, T. B.; May, A. J. *J. Chem. Phys.* **2006**, *124*, 094103.
(68) Schmitz, G.; Hattig, C.; Tew, D. P. *Phys. Chem. Chem. Phys.* **2014**, *16*, 22167−22178.
(69) Tew, D. P.; Hättig, C. *Int. J. Quantum Chem.* **2013**, *113*, 224−229.
(70) Yang, J.; Chan, G. K.-L.; Manby, F. R.; Schütz, M.; Werner, H.-J. *J. Chem. Phys.* **2012**, *136*, 144105.
(71) Schmitz, G.; Helmich, B.; Hättig, C. *Mol. Phys.* **2013**, *111*, 2463−2476.
(72) Schütz, M.; Yang, J.; Chan, G. K.-L.; Manby, F. R.; Werner, H.-J. *J. Chem. Phys.* **2013**, *138*, 054109.
(73) Helmich, B.; Hättig, C. *J. Chem. Phys.* **2011**, *135*, 214106.
(74) Helmich, B.; Hättig, C. *J. Chem. Phys.* **2013**, *139*, 084114.
(75) Helmich, B.; Hättig, C. *Comput. Theor. Chem.* **2014**, *1040−1041*, 35−44.
(76) Demel, O.; Pittner, J.; Neese, F. *J. Chem. Theory Comput.* **2015**, *11*, 3104−3114.
(77) Barr, T. L.; Davidson, E. R. *Phys. Rev. A: At., Mol., Opt. Phys.* **1970**, *1*, 644.
(78) Sosa, C.; Geersten, J.; Trucks, G. W.; Bartlett, R. J.; Franz, J. A. *Chem. Phys. Lett.* **1989**, *159*, 148−154.
(79) Taube, A. G.; Bartlett, R. J. *J. Chem. Phys.* **2008**, *128*, 164101.
(80) Shavitt, I.; Rosenberg, B. J.; Palalikit, S. *Int. J. Quantum Chem.* **1976**, *10*, 33−46.
(81) Russ, N. J.; Crawford, T. D. *J. Chem. Phys.* **2004**, *121*, 691.
(82) Subotnik, J. E.; Head-Gordon, M. *J. Chem. Phys.* **2005**, *123*, 064108.
(83) Mata, R. A.; Werner, H.-J. *J. Chem. Phys.* **2006**, *125*, 184110.
(84) Garavelli, M.; Celani, P.; Bernardi, F.; Robb, M. A.; Olivucci, M. *J. Am. Chem. Soc.* **1997**, *119*, 6891−6901.
(85) Cembran, A.; González-Luque, R.; Serrano-Andrés, L.; Merchán, M.; Garavelli, M. *Theor. Chem. Acc.* **2007**, *118*, 173−183.

DOI: 10.1021/acs.jctc.5b00479
J. Chem. Theory Comput. 2015, 11, 3772−3784

(86) Polli, D.; Altoe, P.; Weingart, O.; Spillane, K. M.; Manzoni, C.; Brida, D.; Tomasello, G.; Orlandi, G.; Kukura, P.; Mathies, R. A.; Garavelli, M.; Cerullo, G. *Nature* **2010**, *467*, 440−443.
(87) Merchán, M.; González-Luque, R.; Climent, T.; Serrano-Andrés, L.; Rodríguez, E.; Reguero, M.; Peláez, D. *J. Phys. Chem. B* **2006**, *110*, 26471−26476.
(88) Giussani, A.; Segarra-Martí, J.; Roca-Sanjuán, D.; Merchán, M. *Top. Curr. Chem.* **2013**, *355*, 57−97.
(89) Rubio, M.; Serrano-Andrés, L.; Merchán, M. *J. Chem. Phys.* **2008**, *128*, 104305.
(90) Segarra-Martí, J.; Roca-Sanjuán, D.; Merchán, M.; Lindh, R. *J. Chem. Phys.* **2012**, *137*, 244309.
(91) Aquilante, F.; de Vico, L.; Ferré, N.; Ghigo, G.; Malmqvist, P.-å; Neogrády, P.; Pedersen, T. B.; Pitoňák, M.; Reiher, M.; Roos, B. O.; Serrano-Andrés, L.; Urban, M.; Veryazov, V.; Lindh, R. *J. Comput. Chem.* **2010**, *31*, 224−247.
(92) Aquilante, F.; Pedersen, T. B.; Veryazov, V.; Lindh, R. *WIRES Comput. Mol. Sci.* **2013**, *3*, 143−149.
(93) Ditchfield, R.; Hehre, W. J.; Pople, J. A. *J. Chem. Phys.* **1971**, *54*, 724.
(94) Widmark, P.-O.; Malmqvist, P.-Å; Roos, B. O. *Theor. Chim. Acta* **1990**, *77*, 291.
(95) Widmark, P.-O.; Persson, B. J.; Roos, B. O. *Theor. Chim. Acta* **1991**, *79*, 419.
(96) Aquilante, F.; Lindh, R.; Bondo Pedersen, T. *J. Chem. Phys.* **2007**, *127*, 114107.
(97) Aquilante, F.; Pedersen, T. B.; Lindh, R. *J. Chem. Phys.* **2007**, *126*, 194106.
(98) Merlot, P.; Kjærgaard, T.; Helgaker, T.; Lindh, R.; Aquilante, F.; Reine, S.; Pedersen, T. B. *J. Comput. Chem.* **2013**, *34*, 1486−1496.
(99) Forsberg, N.; Malmqvist, P.-Å. *Chem. Phys. Lett.* **1997**, *274*, 196−204.
(100) Ghigo, G.; Roos, B. O.; Malmqvist, P.-Å. *Chem. Phys. Lett.* **2004**, *396*, 142−149.
(101) Delcey, M. G.; Freitag, L.; Pedersen, T. B.; Aquilante, F.; Lindh, R.; González, L. *J. Chem. Phys.* **2014**, *140*, 174103.
(102) Klessinger, M.; Michl, J. *Excited States and Photochemistry of Organic Molecules*; VCH Publishers Inc.: New York, 1995.
(103) Lorentzon, J.; Malmqvist, P.-Å; Fülscher, M.; Roos, B. O. *Theor. Chim. Acta* **1995**, *91*, 91−108.
(104) Nenov, A.; Rivalta, I.; Mukamel, S.; Garavelli, M. *Comput. Theor. Chem.* **2014**, *1040−1041*, 295−303.
(105) Nenov, A.; Giussani, A.; Segarra-Martí, J.; Jaiswal, V. K.; Rivalta, I.; Cerullo, G.; Mukamel, S.; Garavelli, M. *J. Chem. Phys.* **2015**, *142*, 212443.
(106) Barbatti, M.; Borin, A. C.; Ullrich, S. *Top. Curr. Chem.* **2014**, *355*, 1−32.
(107) McFarland, B. K.; Farrell, J. P.; Miyabe, S.; Tarantelli, F.; Aguilar, A.; Berrah, N.; Bostedt, C.; Bozek, J. D.; Bucksbaum, P. H.; Castagna, J. C.; Coffee, R. N.; Cryan, J. P.; Fang, L.; Feifel, R.; Gaffney, K. J.; Glownia, J. M.; Martinez, T. J.; Mucke, M.; Murphy, B.; Natan, A.; Osipov, T.; Petrović, V. S.; Schorb, S.; Schultz, T.; Spector, L. S.; Swiggers, M.; Tenney, I.; Wang, S.; White, J. L.; White, W.; Gühr, M. *Nat. Commun.* **2014**, *5*, 4235.
(108) Szalay, P. G.; Watson, T.; Perera, A.; Lotrich, V. F.; Bartlett, R. J. *J. Phys. Chem. A* **2012**, *116*, 6702−6710.
(109) MacLeod, M. K.; Shiozaki, T. *J. Chem. Phys.* **2015**, *142*, 051103.
(110) Page, C. S.; Olivucci, M. *J. Comput. Chem.* **2003**, *24*, 298−309.
(111) Azizi, Z.; Roos, B. O.; Veryazov, V. *Phys. Chem. Chem. Phys.* **2006**, *8*, 2727−2732.
(112) Garavelli, M. *Theor. Chem. Acc.* **2006**, *116*, 87−105.
(113) Valsson, O.; Filippi, C. *J. Chem. Theory Comput.* **2010**, *6*, 1275−1292.
(114) Segarra-Martí, J.; Merchán, M.; Roca-Sanjuán, D. *J. Chem. Phys.* **2012**, *136*, 244306.
(115) Gozem, S.; Huntress, M.; Schapiro, I.; Lindh, R.; Granovsky, A. A.; Angeli, C.; Olivucci, M. *J. Chem. Theory Comput.* **2012**, *8*, 4069−4080.
(116) Gozem, S.; Krylov, A. I.; Olivucci, M. *J. Chem. Theory Comput.* **2013**, *9*, 284−292.
(117) Segarra-Martí, J.; Coto, P. B. *Phys. Chem. Chem. Phys.* **2014**, *16*, 25642−25648.
(118) Tomasello, G.; Olaso-González, G.; Altoè, P.; Stenta, M.; Serrano-Andrés, L.; Merchán, M.; Orlandi, G.; Bottoni, A.; Garavelli, M. *J. Am. Chem. Soc.* **2009**, *131*, 5172−5186.
(119) Polli, D.; Weingart, O.; Brida, D.; Poli, E.; Maiuri, M.; Spillane, K. M.; Bottoni, A.; Kukura, P.; Mathies, R. A.; Cerullo, G.; Garavelli, M. *Angew. Chem., Int. Ed.* **2014**, *53*, 2504−2507.
(120) Segarra-Martí, J.; Coto, P. B.; Rubio, M.; Roca-Sanjuán, D.; Merchán, M. *Mol. Phys.* **2013**, *111*, 1308−1315.
(121) Crespo-Hernández, C. E.; Cohen, B.; Hare, P. M.; Kohler, B. *Chem. Rev.* **2004**, *104*, 1977−2020.
(122) Canuel, C.; Mons, M.; Piuzzi, F.; Tardivel, B.; Dimicoli, I.; Elhanine, M. *J. Chem. Phys.* **2005**, *122*, 074316.
(123) Hudock, H. R.; Levine, B. G.; Thompson, A. L.; Satzger, H.; Townsend, D.; Gador, N.; Ullrich, S.; Stolow, A.; Martínez, T. J. *J. Phys. Chem. A* **2007**, *111*, 8500−8508.
(124) Yamazaki, S.; Taketsugu, T. *J. Phys. Chem. A* **2012**, *116*, 491−503.
(125) Barbatti, M.; Aquino, A. J. A.; Szymczak, J. J.; Nachtigallová, D.; Hobza, P.; Lischka, H. *Proc. Natl. Acad. Sci. U. S. A.* **2010**, *107*, 21453−21458.
(126) Buchner, F.; Nakayama, A.; Yamazaki, S.; Ritze, H.-H.; Lübcke, A. *J. Am. Chem. Soc.* **2015**, *137*, 2931−2938.
(127) Nakayama, A.; Arai, G.; Yamazaki, S.; Taketsugu, T. *J. Chem. Phys.* **2013**, *139*, 214304.
(128) Altavilla, S. F.; Segarra-Martí, J.; Nenov, A.; Conti, I.; Rivalta, I.; Garavelli, M. *Front. Chem.* **2015**, *3*, 29.
(129) Gonzalez-Vazquez, J.; Gonzalez, L.; Samoylova, E.; Schultz, T. *Phys. Chem. Chem. Phys.* **2009**, *11*, 3927−3934.
(130) Picconi, D.; Barone, V.; Lami, A.; Santoro, F.; Improta, R. *ChemPhysChem* **2011**, *12*, 1957−1968.
(131) Picconi, D.; Lami, A.; Santoro, F. *J. Chem. Phys.* **2012**, *136*, 244104.
(132) Roberts, G. M.; Stavros, V. G. *Chem. Sci.* **2014**, *5*, 1698−1722.
(133) Roberts, G. M.; Hadden, D. J.; Bergendahl, L. T.; Wenge, A. M.; Harris, S. J.; Karsili, T. N. V.; Ashfold, M. N. R.; Paterson, M. J.; Stavros, V. G. *Chem. Sci.* **2013**, *4*, 993−1001.
(134) Wells, K. L.; Hadden, D. J.; Nix, M. G. D.; Stavros, V. G. *J. Phys. Chem. Lett.* **2010**, *1*, 993−996.
(135) Sobolewski, A. L.; Domcke, W. *Chem. Phys.* **2000**, *259*, 181−191.
(136) Sobolewski, A. L.; Domcke, W. *Phys. Chem. Chem. Phys.* **2002**, *4*, 4−10.
(137) Olaso-González, G.; Roca-Sanjuán, D.; Serrano-Andrés, L.; Merchán, M. *J. Chem. Phys.* **2006**, *125*, 231102.
(138) Aquino, A. J. A.; Nachtigallova, D.; Hobza, P.; Truhlar, D. G.; Hättig, C.; Lischka, H. *J. Comput. Chem.* **2011**, *32*, 1217−1227.
(139) Chipman, D. M. *J. Chem. Phys.* **2006**, *124*, 044305.
(140) Braams, B. J.; Bowman, J. M. *Int. Rev. Phys. Chem.* **2009**, *28*, 577−606.

DOI: 10.1021/acs.jctc.5b00479
J. Chem. Theory Comput. 2015, 11, 3772−3784